

Robust Optimal Output-tracking Control of Constrained Mechanical Systems with Application to Autonomous Rovers

Mohammadreza Mottaghi, Robin Chhabra, *Member, IEEE*

Abstract—This paper presents a robust optimal output-tracking control strategy for underactuated mechanical systems whose motion is restricted by mixed holonomic and nonholonomic constraints. Autonomous rovers/cars and unmanned underwater/aerial vehicles are a few examples of such systems that must often operate in harsh environments and under uncertain conditions. We present a comprehensive control analysis of this large class of nonlinear systems, including the existing studies on local reachability and static state feedback linearization. We also propose a local observability analysis of the feedback transformed input-output linearized systems. Based on the input-output linearization of the holonomically restricted nominal system, we develop a sliding mode control strategy that is robust against projected effects of uncertainties and disturbances on the system's output. Asymptotic stability of the output towards a bounded desired trajectory is proved using Lyapunov's direct method while the system's internal stability (in the sense of boundedness) is investigated based on the notion of tracking-error zero dynamics. Time-dependent bounded matched uncertainties in the inertia parameters and disturbance forces arising in the unrestricted system are considered in this study. We propose an optimal sliding manifold according to the finite-horizon linear-quadratic regulator design problem with split boundary value conditions. The developed control strategy is implemented on a six-wheel autonomous Lunar rover in a simulation environment and its performance is compared with that of an optimal proportional-integral-derivative feedback, feedforward controller. The optimal sliding mode controller shows superior performance in trajectory tracking with acceptable control actions.

Index Terms—Robust Output-tracking, Feedback Linearization, Nonholonomic Mechanics, Sliding Mode Control, Optimal Control.

I. INTRODUCTION

CONSTRAINED robotic systems play a central role in many modern applications, such as space exploration, search and rescue, and aerial package delivery. Such systems inherent complex dynamics and due to their mission requirements they must operate autonomously under uncertain and hostile conditions. Thus, robustness is a crucial factor that should be considered in the design of their control systems.

Presence of constraints in mechanical systems, particularly nonholonomic (non-integrable) ones, introduces modelling and

control challenges, e.g., underactuation and loss of full-state feedback linearizability property [1]. Several comprehensive frameworks have been presented to capture the behaviour of mechanical systems with constraints, specially in Pfaffian form [2], [3]. In [4], a unified dynamical model of robotic systems subject to nonlinear constraints is outlined that is based on differential variational principles. Yun and Sarkar unify the state space representation of systems subject to mixed holonomic (integrable) and nonholonomic constraints via substituting algebraic holonomic equations by stable first-order differential equations to improve the stability of numerical simulations [5]. Control challenges associated with nonholonomic systems, such as motion planning and feedback stabilization, are well-documented in the literature [6], [7]. A geometric exposition on nonholonomic control is presented in a book by Bloch that includes studying symmetry properties, optimal control and energy-based methods of stabilization of nonholonomic systems [8]. An optimal point stabilization control of nonholonomic systems is proposed based on an affine connection formulation [9]. Trajectory stabilization of nonholonomic systems has been also addressed using, e.g., a linearized model of system around a trajectory [10] or applying optimal control theory and Pontryagin maximum principle [11]. Further, output-tracking control laws for mechanical systems with nonholonomic rolling constraints have been developed based on input-output linearization techniques [12]. Chhabra *et al.* propose an output-tracking control strategy for symmetric nonholonomic Hamiltonian systems [13], founded upon their dynamical reduction [14] and input-output linearization in their reduced state space, applying static state feedback. This technique is implemented to design a torque-based controller for the Lunar Exploration Light Rover [15].

In reference to robust control of nonlinear systems, various techniques including integral control, Sliding Mode Control (SMC), and gain scheduling are discussed in a book by Khalil [16]. Nonlinear robust controllers can be also designed applying exogenous disturbance observers and adaptive control laws under the assumption that the uncertain dynamics can be estimated [17], [18]. Sliding mode control, as a robust variable structure control strategy, has been employed in many control applications, due to its simple structure, guaranteed asymptotic stability, and introduction of reduced order error dynamics [19]. To improve the performance of SMC, a chattering-free SMC is derived based on a time varying feedback gain, whose global stability is proven using the Lyapunov second theorem

M.R. Mottaghi and R. Chhabra are with the Mechanical and Aerospace Engineering department, Carleton University, Ottawa, Canada (e-mail: mohammadreza.mottaghi@carleton.ca, robin.chhabra@carleton.ca)

and invariance principle [20]. In [21] using output feedback and applying SMC to the input-output dynamics, a robust output tracking control law is proposed along with a time-dependant exponent parameter law to ensure both accuracy and low energy consumption. Ge *et al.* propose a robust adaptive state/output feedback point stabilization of a class of nonholonomic systems in chained form along with an adaptive switching law guaranteeing the boundedness of the states [22]. For systems subject to holonomic and nonholonomic constraints, a systematic robust motion/force control law is developed based on an online adaptive parameter estimation [23]. A robust control scheme has also been developed for stabilization of nonholonomic systems with drift uncertainties, using time-varying SMC [24].

A category of mechanical systems that are subject to both holonomic and nonholonomic constraints is autonomous planetary exploration rovers that often experience several forms of uncertainties and disturbances [25]. The evolution of control systems developed for nonholonomic rovers initiated in 1990s. The full posture kinematic tracking control of Differential Drive Rovers (DDRs), based on Lyapunov design, is proposed in [26]. This result was extended to include robustness by designing a SMC in polar coordinates for DDRs experiencing unknown disturbing forces [27]. Ashrafiuon *et al.* develop a SMC for uncertain simple planar vehicles with only two control inputs that is robust against bounded time-dependant matched uncertainties. This method is based on a reduced order error dynamics obtained using the concept of transitional trajectory [28]. State feedback linearization of different types of rover systems has been also investigated, applying static or dynamic state feedback [29]. Wang and Xu propose a set of output functions for which rover systems are input-output linearizable applying static state feedback [30].

This paper presents a complete control analysis for a class of constrained mechanical systems that are subject to both holonomic and nonholonomic constraints in Pfaffian form. We extend the local reachability investigation discussed in [31] to general constrained systems, and collect different analyses on feedback linearizability and output-tracking control performed in [16], [30]–[32]. Additionally, we investigate the observability properties of such systems after applying an input-output linearizing feedback transformation. The main objective of this paper is to develop a robust optimal output-tracking control strategy for this class of mechanical systems, by input-output linearizing the nominal plant. Time-dependent matched uncertainties in inertia parameters and disturbance forces arising in the unrestricted dynamics of the system are considered. We propose a SMC with an optimally designed sliding manifold to increase the robustness of the output-tracking control task against projected effects of uncertainties and disturbances on the system's output. We obtain the sliding manifold by solving a Linear-Quadratic Regulator (LQR) design problem with split boundary value conditions. The error dynamics on the optimal sliding manifold follows a Proportional-Integral-Derivative (PID) control law, whose integral term also helps with the robustness of the system. Using the Lyapunov's direct method, we prove the asymptotic stability of the output error towards the origin. Further, we show the asymptotic stability of the

observable internal states and boundedness of the unobservable internal states applying the concept of tracking-error zero dynamics. To alleviate the chattering effects associated with the developed SMC, we used the method of boundary layer proposed in [16], [33] and substitute the sign function in the switching control law by a high-slope continuous saturation function. The major contributions of this paper are as follows:

- (i) We propose an observability decomposition of the internal states of constrained mechanical control systems that is used in the stability analysis of the internal dynamics.
- (ii) We develop a robust output-tracking SMC strategy that is applicable to a wide range of constrained mechanical systems experiencing complex bounded time-dependent matched uncertainties in their inertia parameters.
- (iii) We design an optimal sliding manifold at the output level that minimizes a functional based on a norm square of the output error and that of the control actions.

The developed control strategy is implemented on a six-wheel type (1;1) autonomous rover that is designed for future Lunar exploration missions. Uncertainties in the form of added moving mass, variable moment of inertia, unbalanced wheel, and time-varying external forces are considered in the control design of the rover. We demonstrate the efficacy of the proposed optimal SMC thorough showing its superior performance in comparison to that of an optimally designed output-tracking PID feedback, feedforward controller. Note that the results of this paper can be directly applied to robotic systems, including autonomous cars and underwater/aerial vehicles, with 2- dimensional planar mobility.

The outline of the paper is as follows. Section II discusses the dynamical modelling of constrained mechanical systems with both holonomic and nonholonomic constraints. In Section III, various control aspects and state decompositions of constrained mechanical systems are studied. The proposed optimal robust output-tracking control algorithm is detailed in Section IV. Finally, the developed theory is implemented on a six-wheel autonomous Lunar rover in section V. Section VI provides some concluding remarks.

II. CONSTRAINED MECHANICAL SYSTEMS

In this section, we describe a class of mechanical control systems with mixed holonomic and nonholonomic constraints. We consider the evolution of such systems in the tangent bundle of their n -dimensional smooth configuration manifold, denoted by \hat{Q} . A set of r everywhere linearly independent constraints on velocities in Pfaffian form is considered:

$$\hat{A}(\mathbf{q})\dot{\mathbf{q}} = 0; \quad (1)$$

where $(\mathbf{q}; \dot{\mathbf{q}}) \in T\hat{Q}$, the tangent bundle of the configuration manifold, and $\hat{A} : \hat{Q} \rightarrow \mathbb{R}^{r \times n}$ is the constraint matrix. All admissible velocities of the system must lie in the $(n - r)$ -dimensional annihilator distribution D resulted from the constraint equations. Let $\hat{N} : \hat{Q} \rightarrow \mathbb{R}^{n \times r}$ denote the matrix whose columns span D , i.e., $\hat{A}(\mathbf{q})\hat{N}(\mathbf{q}) = 0$.

Assumption 1. We assume that there exists a choice of \hat{N} which is everywhere full-rank on \hat{Q} .

Based on the Lagrange d'Alembert principle, dynamics of the constrained mechanical system is derived in matrix form:

$$\hat{M}(\mathbf{q})\dot{\mathbf{q}} + \hat{C}(\mathbf{q}; \dot{\mathbf{q}})\dot{\mathbf{q}} + \hat{\mathbf{g}}(\mathbf{q}) = \hat{B}(\mathbf{q})\mathbf{u} + \hat{A}(\mathbf{q})^T \boldsymbol{\lambda}; \quad (2)$$

where $\hat{M} : \hat{Q} \rightarrow \mathbb{R}^{n \times n}$ is the symmetric positive definite mass matrix of the system, $\hat{C} : T\hat{Q} \rightarrow \mathbb{R}^{n \times n}$ is the matrix of Coriolis and centrifugal forces, $\hat{\mathbf{g}} : \hat{Q} \rightarrow \mathbb{R}^n$ is the vector of potential forces, $\mathbf{u} \in \mathbb{R}^s$ is the vector of control inputs, $\hat{B} : \hat{Q} \rightarrow \mathbb{R}^{n \times s}$ is the matrix whose columns are the control directions, and $\boldsymbol{\lambda} \in \mathbb{R}^r$ is the vector of Lagrange multipliers. Hereinafter, for brevity the dependency of the matrices and vectors is dropped wherever it does not raise confusion.

Assumption 2. The dimension of the vector $\boldsymbol{\lambda}$ is greater than or equal to the dimension of distribution D , i.e., $s \geq n - r$, and no columns of \hat{B} are in the image of \hat{A} .

If the involutive closure of D , denoted by \bar{D} , is of system's dimension (\bar{n}), then all imposed constraints are nonholonomic (non-integrable). The involutive closure of D is the minimal distribution that contains elements of D and all iterative Lie-brackets of vector fields in D . If the dimension of \bar{D} is equal to $n = \bar{n} - p$, the system experiences p holonomic (integrable) constraints and $m = r - p$ nonholonomic constraints.

After identifying the holonomic constraints, we introduce the restricted configuration manifold Q , with dimension n , which is an embedded sub-manifold of \hat{Q} with the inclusion map $\iota : Q \rightarrow \hat{Q}$. In other words, Q is the maximal integral manifold of the holonomic distribution. Let $(\mathbf{q}; \dot{\mathbf{q}}) \in TQ$ denote an element of the tangent bundle of Q , and let $J(\mathbf{q})$ be the Jacobian of the inclusion map. The set of m remaining completely nonholonomic constraints on Q are defined by:

$$A(\mathbf{q})\dot{\mathbf{q}} = 0; \quad (3)$$

where

$$A(\mathbf{q}) = E\hat{A}(\iota(\mathbf{q}))J(\mathbf{q}); \quad (4)$$

Due to inclusion of holonomic constraints, the rows of the matrix $\hat{A}J$ are linearly dependant and they span a co-distribution of dimension m . Here, the constant matrix $E \in \mathbb{R}^{m \times r}$ introduces a minimal linear combination of the rows of $\hat{A}J$ to parameterize the resultant co-distribution, which eliminates the redundant constraint directions.

Pre-multiplying both sides of (2) by $J^T(\mathbf{q})$, and substituting $\dot{\mathbf{q}}$ and $\boldsymbol{\lambda}$, based on the inclusion map, i.e.,

$$\begin{aligned} \dot{\mathbf{q}} &= J(\mathbf{q})\dot{\mathbf{q}}; \\ \boldsymbol{\lambda} &= J(\mathbf{q}; \dot{\mathbf{q}})\dot{\mathbf{q}} + J(\mathbf{q})\boldsymbol{\lambda}; \end{aligned} \quad (5)$$

where

$$J(\mathbf{q}; \dot{\mathbf{q}}) = \sum_{j=1}^n \frac{\partial J(\mathbf{q})}{\partial \dot{\mathbf{q}}_j} \dot{\mathbf{q}}_j;$$

is the time derivative of the matrix J , the equations of motion in the restricted configuration manifold Q become:

$$M(\mathbf{q})\dot{\mathbf{q}} + C(\mathbf{q}; \dot{\mathbf{q}})\dot{\mathbf{q}} + \mathbf{g}(\mathbf{q}) = B(\mathbf{q})\mathbf{u} + A(\mathbf{q})^T \boldsymbol{\lambda}; \quad (6)$$

Here, \mathbf{q}_j denotes the j^{th} element of \mathbf{q} , $N : Q \rightarrow \mathbb{R}^{n \times m}$ is a matrix whose columns span the null-space of the constraint matrix A (The existence of everywhere full-rank matrix N can be directly deduced from Assumption 1 and the fact that Q is an embedded submanifold of \hat{Q} , and $\mathbb{R}^{n \times m}$ is the vector of quasi-velocities, $M := J^T \hat{M}(\iota(\mathbf{q}))J$ is the mass matrix, $C := J^T (\hat{M}(\iota(\mathbf{q}))\dot{J} + \hat{C}(\iota(\mathbf{q}); J\dot{\mathbf{q}}))J$ is the matrix of Coriolis and centrifugal forces, $\mathbf{g} := J^T \hat{\mathbf{g}}(\iota(\mathbf{q}))$ is the vector of potential forces, $B := J^T \hat{B}(\iota(\mathbf{q}))$ is the matrix of control directions, and $\boldsymbol{\lambda} := E^T \boldsymbol{\lambda} \in \mathbb{R}^m$ is the vector of Lagrange multipliers.

Remark 1. In this paper, we define an explicit restriction of the system's states to a maximal integral manifold of the distribution corresponding to holonomic constraints, since uncertainties and control inputs are all originally applied in the unrestricted configuration manifold.

Pre-multiplying both sides of the set of equations representing the dynamics of the system in (6) by N^T , and substituting

$$\begin{aligned} \dot{\mathbf{q}} &= N(\mathbf{q}; \dot{\mathbf{q}}) + N(\mathbf{q})\boldsymbol{\lambda}; \\ N(\mathbf{q}; \dot{\mathbf{q}}) &= \sum_{j=1}^n \frac{\partial N(\mathbf{q})}{\partial \dot{\mathbf{q}}_j} \dot{\mathbf{q}}_j; \end{aligned} \quad (7)$$

the set of equations on the state space of the system $X \subset TQ$, which is the distribution spanned by the columns of N , is obtained as:

$$\begin{aligned} \dot{\mathbf{q}} &= N(\mathbf{q})\boldsymbol{\lambda}; \\ M_r(\mathbf{q})\dot{\mathbf{q}} + C_r(\mathbf{q}; \dot{\mathbf{q}})\dot{\mathbf{q}} + \mathbf{g}_r(\mathbf{q}) &= B_r(\mathbf{q})\mathbf{u}; \end{aligned} \quad (8)$$

Here, given $N^T A^T = 0$, the constraint forces are eliminated, and

$$\begin{aligned} M_r &:= N^T M N; \\ C_r &:= N^T (M N(\mathbf{q}; N\dot{\mathbf{q}}) + C(\mathbf{q}; N\dot{\mathbf{q}})N); \\ B_r &:= N^T B; \\ \mathbf{g}_r &:= N^T \mathbf{g}; \end{aligned}$$

are respectively the reduced mass matrix, the reduced matrix of Coriolis and centrifugal forces, the reduced matrix of control directions, and the reduced vector of potential forces.

We denote a member of X by $\mathbf{x} = [\mathbf{q}^T; \dot{\mathbf{q}}^T]^T$ that is a $(2n - m)$ -dimensional vector of system states. The state space representation of the governing equations of motion is

$$\dot{\mathbf{x}} = \mathbf{f}(\mathbf{x}) + G(\mathbf{x})\mathbf{u}; \quad (9)$$

where

$$\mathbf{f}(\mathbf{x}) = \begin{bmatrix} N \\ M_r^{-1}(C_r + \mathbf{g}_r) \end{bmatrix}; \quad G(\mathbf{x}) = \begin{bmatrix} \mathbf{0}_{n \times s} \\ M_r^{-1}B_r \end{bmatrix}; \quad (10)$$

and $\mathbf{0}$ denotes the matrix of zeros with proper dimensions.

III. CONTROL ANALYSIS

In this section, we provide a compendious control analysis of the system in (9). First, the full-state reachability and feedback linearizability are studied applying the tools presented in [32] to the category of constrained mechanical systems in (9). Then, the studies in [30], [31] are generalized to the systems

represented by (9) to investigate their input-output linearizability and the stability of their internal dynamics. Finally, we propose an observability decomposition of the internal states to improve the existing stability analysis presented in [30].

A. Reachability and Full-state Feedback Linearizability

Let us introduce the control input $u \in \mathbb{R}^{n-m}$, based on

$$B_r = C_r + g_r + M_r ; \quad (11)$$

that partially linearizes the system in (9). Under this transformation, the resultant closed-loop system becomes

$$\begin{aligned} \dot{x} &= f^1(x) + G^1 u ; \\ f^1(x) &= \begin{bmatrix} N \\ O_{(n-m) \times 1} \end{bmatrix} ; \quad G^1 = \begin{bmatrix} O_{n \times (n-m)} \\ I_{(n-m) \times (n-m)} \end{bmatrix} ; \end{aligned} \quad (12)$$

where I denotes the identity matrix with appropriate dimensions.

The control system in (12) is fully reachable if and only if for any arbitrary pair of an initial state x_0 and a terminal state x_f , one can find a control input moving the system from x_0 to x_f .

Proposition 1. The control system in (9) is fully locally reachable.

Proof: Let H be a family of nonsingular involutive distributions containing the columns of G^1 and being invariant under the drift vector field $f^1(x)$ and the columns of G^1 . The family of distributions H has a minimal element [32]. We denote the minimal element of H by H_0 that has dimension d . At each state x_0 there is an open neighbourhood $U_0 \subset \mathbb{R}^{2n-m}$ of x_0 on which H_0 defines a foliation of embedded d -dimensional slices in U_0 . The slice containing x_0 is the set of all states that are reachable along trajectories of the system starting from x_0 and staying in U_0 . This slice is called the reachable set from x_0 and it is denoted by $R_{x_0} \subset U_0$. Consequently, the system in (12) is fully locally reachable, and only if H_0 is of system's dimension, i.e. $d = 2n - m$ [32].

To construct H_0 for the system in (12), first the distribution spanned by the columns of matrix G^1 is considered. Then, the invariance condition of H_0 under the drift vector field $f^1(x)$ is imposed that results in the distribution

$$K := \text{im}(G^1) + \text{span}\{L_{f^1} G_j^1, j = 1, \dots, n-m\}; \quad (13)$$

Here, G_j^1 is the j th column of G^1 . The Lie derivatives in (13) are computed as:

$$L_{f^1} G_j^1 = \frac{\partial G_j^1}{\partial x} f^1 = \frac{\partial G_j^1}{\partial x} \begin{bmatrix} N \\ O_{(n-m) \times 1} \end{bmatrix}; \quad (14)$$

Since G_j^1 is constant based on (12) $\frac{\partial G_j^1}{\partial x} = 0$. Additionally, based on (12) $f^1 = \begin{bmatrix} N \\ O_{(n-m) \times 1} \end{bmatrix}$ where N is only a function of q ; hence, we have:

$$L_{f^1} G_j^1 = \begin{bmatrix} \frac{\partial N}{\partial q} \\ O_{(n-m) \times (n)} \end{bmatrix} \begin{bmatrix} N \\ O_{(n-m) \times (n-m)} \end{bmatrix} G_j^1;$$

Accordingly, since the first rows of G^1 are equal to zero, $K = \text{im}(G^1) + \text{im} \begin{bmatrix} N \\ O_{(n-m) \times (n-m)} \end{bmatrix}$; (15)

which is of dimension $2n - 2m$. Note that the distribution K defined in (15), indicates the evolution of the system in the direction of its control inputs and drift vector field. Finally, the involutivity condition is considered in construction of H_0 . Since we assumed completely nonholonomic constraints in (3), the involutivity condition of H_0 adds m new directions when considering the Lie Brackets of vector fields in K . Therefore, based on dimension counting the dimension of H_0 is equal to that of the system, and (12) is fully locally reachable. Since the system in (12) is a special case of the system in (9), its fully locally reachability can be extended to the system in (9).

Reachability is the necessary condition for local controllability. A fully locally reachable system is locally controllable assuming that every initial state x_0 is in the interior of the reachable set R_{x_0} [34].

Assumption 3. The system in (12) and hence the system in (9) is locally controllable.

Proposition 2. The system in (9) is not full-state feedback linearizable by a smooth state feedback.

Proof: A nonlinear control system is full-state feedback linearizable applying a smooth state feedback if and only if it is fully locally reachable and also a nested sequence of distributions defined by

$$F_k := \text{span}\{L_{f^1}^i G_j^1, i = 0, \dots, k-1; j = 1, \dots, n-m\}; \quad (16)$$

for $k = 1, 2, \dots$, are all involutive and constant dimensional [35]. G_j denotes the j th column of matrix G . The distribution F_2 is

$$\begin{aligned} F_2 &= \text{im}(G) + \text{span}\{L_{f^1} G_j^1, j = 1, \dots, n-m\}; \\ &= \text{im}(G) + \text{im} \begin{bmatrix} N M_r^{-1} B_r \\ W(q) \end{bmatrix}; \end{aligned} \quad (17)$$

where $W : Q \rightarrow \mathbb{R}^{(n-m) \times s}$ is a vector function determined by calculation of $L_{f^1} G_j$ using the Lie derivative equation in (14). Note that the step by step procedure of calculating F_k is similar to computations performed for obtaining K in the proof of Proposition 1 and hence it is omitted here. Based on Assumption 2 and the positive definiteness of M , the matrix $M_r^{-1} B_r$ is full-rank. Consequently, $\text{im}(G)$ covers all directions tangent to quasi velocities and $\text{im} \begin{bmatrix} N \\ W(q)^T \end{bmatrix} \subset \text{im}(G)$. Accordingly, if F_2 is involutive, then $\text{im}(N)$ must be involutive. Due to the nonholonomicity of the constraints the distribution $\text{im}(N)$ is not involutive and that completes the proof.

B. Input-Output Linearization and Output Tracking

Let the b -dimensional vector $y \in \mathbb{R}^b$ denote the output of the system in (12). We define the relationship between the states and the output of the system with the smooth function

$$\begin{aligned} h : Q &\rightarrow \mathbb{R}^b \\ q &\rightarrow y = h(q); \end{aligned} \quad (18)$$

The relationship between the control input and the component of the output is obtained by:

$$\begin{aligned} y_i &= L_x h_i = L_{f^1} h_i; \\ \dot{y}_i &= L_x^2 h_i = L_{f^1}^2 h_i + L_{G^1} L_{f^1} h_i; \end{aligned} \quad (19)$$

The Lie derivatives in (19) are calculated as:

$$L_{f^1} h_i = \left(\frac{\partial h_i}{\partial x} \right)^T f^1 = \left(\frac{\partial h_i}{\partial x} \right)^T N; \quad (20)$$

$$\begin{aligned} L_{f^1}^2 h_i &= \frac{\partial (L_{f^1} h_i)}{\partial x} \cdot f^1 = \left(\frac{\partial}{\partial x} \right)^T N^T \frac{\partial h_i}{\partial x^2} N \\ &+ \sum_{j=1}^m \left(\frac{\partial h_i}{\partial x} \right)^T \frac{\partial}{\partial x} N_j; \end{aligned} \quad (21)$$

$$L_{G^1} L_{f^1} h_i = \left(\frac{\partial h_i}{\partial x} \right)^T N; \quad (22)$$

where N_j denotes the j^{th} column of the matrix N , N_j is the j^{th} component of the vector, $\frac{\partial}{\partial x}$ is the Jacobian of a scalar or vector function, and $\frac{\partial^2}{\partial x^2}$ denotes the Hessian of a scalar function.

Let us define the input-output decoupling matrix

$$F := \frac{\partial h}{\partial x} N; \quad (23)$$

and the vector function $w : X \rightarrow \mathbb{R}^b$, whose i^{th} component is given in (21). Then, the input-output map is described by:

$$\dot{y} = w + F u; \quad (24)$$

Assumption 4. Hereinafter, the dimension of the output equals to the difference between the dimension of the system and the number of completely nonholonomic constraints. i.e., $b = n - m$. Hence the decoupling matrix F is square.

Assumption 5. The decoupling matrix F is everywhere nonsingular.

Remark2. Since the output is a smooth function and based on Assumption 3 and 5, the system in (9) along with the output defined in (18) is locally input-output controllable.

Proposition 3. Based on Assumption 4 and 5, the system in (9) along with the output defined in (18) is input-output linearizable with relative degree 2, applying a static state feedback.

Proof: Based on Assumption 4 and 5, the decoupling matrix F is everywhere invertible and hence the system in (12) along with the output in (18) is input-output linearizable applying the static state feedback:

$$(x; u) = F^{-1}(q)(u - w); \quad (25)$$

where the vector $w \in \mathbb{R}^b$ denotes the vector of control inputs in the resulting closed loop system. Under this feedback transformation, the input-output relation is in the form of a double integrator.

$$\dot{y} = u; \quad (26)$$

Clearly, the control input obtained from substitution of (25) in (11) results in the same input-output linearized system in (26) for the system in (9).

Remark3. All analyses presented in this paper are under the assumption that the output function has been specially selected in a manner that Assumptions 4 and 5 are satisfied.

In (26) we introduce the external dynamics of the system in (9) along with the output in (18), applying the feedback transformation in (25) and (11). Hence, the state space can be partitioned into the b -dimensional space of external states denoted by $Z_2 \times X$ (the space of output and its velocity) and an $(n - b)$ -dimensional space of the internal states, denoted by Z_1 . The external states $z_2 \in Z_2$ are in the following form:

$$z_2 = y^T \quad \dot{y}^T{}^T; \quad (27)$$

The components of the internal states z_1 are obtained as $n - b$ arbitrary real valued functions $z_{1i} : X \rightarrow \mathbb{R}$ satisfying two conditions: (i) the coordinate transformation mapping $X \rightarrow Z_1 \times Z_2$ that maps x to the vector $z = [z_1^T; z_2^T]^T$ must be a local diffeomorphism, and (ii) the dynamics of the internal states must be independent of, i.e.,

$$\left(\frac{\partial z_{1i}}{\partial x} \right)^T G = 0 \quad i = 1; \dots; n - b; \quad (28)$$

Proposition 4. Real-valued functions z_{1i} locally exist for the system in (9) with the output in (18).

Proof: This proposition is a direct consequence of Theorem 13.1 in [16].

The internal/external state decomposition (known as the normal form) for the system in (9) is expressed as:

$$\begin{aligned} \dot{z}_1 &= f(z_1; z_2); \\ \dot{z}_2 &= A_c^2 z_2 + B_c^2 u; \end{aligned} \quad (29)$$

where the i^{th} component of f is

$$\dot{z}_{1i} = \frac{\partial}{\partial x} f_i(T^{-1}(z)) \quad ; \quad i = 1 \dots n - b; \quad (30)$$

and $A_c^2 \in \mathbb{R}^{2b \times 2b}$ and $B_c^2 \in \mathbb{R}^{2b \times b}$ are the constant matrices representing the canonical form of a chain of two integrators.

A local diffeomorphism as a state transformation can also be defined to partition the space of internal states into: (i) the

a -dimensional space $Z_1^o \subset Z_1$ containing the observable internal states from the output in (18) for the control system in (9), and (ii) $(n - b - a)$ -dimensional space $Z_1^u \subset Z_1$ containing the states that are unobservable from the output in (18) for both control systems in (29) and (9). Let us consider the elements $z_1^o \in Z_1^o$ and $z_1^u \in Z_1^u$. Based on this decomposition, the system in (29) can be further transformed to

$$\begin{aligned} \dot{z}_1^u &= f^u(z_1^u; z_1^o; z_2); \\ \dot{z}_1^o &= f^o(z_1^o; z_2); \\ \dot{z}_2 &= A_c^2 z_2 + B_c^2 u; \end{aligned} \quad (31)$$

where the functions f^u and f^o describe the dynamics of the observable and unobservable internal states, respectively.

Remark4. Given the fact that the observability decomposition is dependent on the output function, this decomposition is discussed in details in Section V for a specific output function.

We denote the desired trajectories for the external states by $z_{2d}(t)$, for the observable internal states $z_{1d}^o(t)$, and for the

unobservable internal states $z_{1e}^u(t)$, where $2 \mathbb{R}^+$ refers to time.

Remark 5. Based on Assumption 3, the system in (9) is not kinematically redundant. Hence $z_{1d}^o(t)$ and $z_{1d}^u(t)$ are uniquely determined based on $z_{2d}(t)$ and the initial configuration of the system, applying the set of kinematic equations in (6).

The tracking error dynamics of the system in (31) can be formed as

$$\begin{aligned} z_{1e}^u &= !_e^u(z_{1e}^u; z_{1e}^o; z_{2e}; t); \\ z_{1e}^o &= !_e^o(z_{1e}^o; z_{2e}; t); \\ z_{2e} &= A_c z_{2e} + B_c v; \end{aligned} \quad (32)$$

where $z_{1e}^o := z_1^o - z_{1d}^o(t)$ is the tracking error of the observable internal states, $z_{1e}^u := z_1^u - z_{1d}^u(t)$ is the tracking error of the unobservable internal states, $z_{2e} := z_2 - z_{2d}$ is the tracking error of the external states and $v := u - \dot{y}_d(t)$. The functions $!_e^u$ and $!_e^o$ respectively describe the error dynamics of the observable and unobservable internal states, based on (31).

Remark 6. Since the elements z_{1e}^u are not affecting the output in (18) for the control system in (9), their asymptotic stability in an output-tracking control problem is of less importance as long as they are bounded.

Problem 1 (Output-tracking Control Problem) Given a twice differentiable desired feasible trajectory $y_d(t)$ for the output of the system, find a control law that tracks $z_{2d}(t)$ with an asymptotically stable tracking error z_{2e} and z_{1e}^o , and a bounded tracking error z_{1e}^u .

The stability of the tracking error for the elements of z_{1e}^o can be investigated based on the concept of tracking-error zero dynamics. The tracking-error zero dynamics is the error dynamics of the internal states when the output error is kept identically zero applying an appropriate control input. Accordingly, the tracking-error zero dynamics of (31) is

$$z_{1e}^o = !_e^o(z_{1e}^o; 0; t); \quad (33)$$

Assumption 6. The function $!_e^o$ is locally Lipschitzian in $(z_{1e}^o; z_{2e})$, uniformly with respect to $t \geq 0$.

Proposition 5. If the tracking-error zero dynamics in (33) is locally uniformly asymptotically stable, then z_{1e}^o is locally uniformly asymptotically stable, after determining as a solution of output tracking control problem.

Proof: Considering Assumption 6, this proposition is the direct consequence of lemma B.2.4 on page 514 in [32].

Assumption 7. We assume that the tracking error z_{1e}^u is bounded, if the tracking error z_{2e} and z_{1e}^o are both locally uniformly asymptotically stable and the desired trajectories are bounded.

IV. ROBUST OPTIMAL OUTPUT-TRACKING CONTROL

An input-output feedback linearized control system in (29) is only valid if all system's parameters are completely known and system is not subject to any disturbances. In this section, a control algorithm is proposed based on Sliding Mode Control

(SMC) scheme to ensure robustness against bounded time-dependant matched uncertainties in the inertia parameters and disturbance forces.

Assumption 8. In this paper, perfect sensory data acquisition and complete knowledge of kinematic (geometric) parameters of the system is assumed.

Let us introduce a time-dependent n -dimensional vector of uncertain inertia parameters and disturbance forces in a bounded neighbourhood \mathbb{R}^c , i.e., $! : \mathbb{R}^+ \rightarrow \mathbb{R}^c$. In the mechanical system described in (2), the uncertainties appear in the form of addition of uncertain terms $\hat{M} : \mathbb{Q} \rightarrow \mathbb{R}^{n \times n}$, $\hat{C} : \mathbb{TQ} \rightarrow \mathbb{R}^{n \times 1}$, and $\hat{g} : \mathbb{Q} \rightarrow \mathbb{R}^n$ to the mass matrix, Coriolis matrix, and the vector of potential forces, respectively. We consider disturbance forces in the following form

$$\hat{f} = \sum_{i=1}^{N_v} J_{di} \hat{f}_i; \quad (34)$$

where \hat{f}_i are functions of time and $J_{di} : \mathbb{Q} \rightarrow \mathbb{R}^n$ are the directions of disturbance forces. Accordingly, the uncertain state space representation of the system in (9) is

$$\dot{x} = f_u(x) + G_u(x); \quad (35)$$

where

$$f_u(x) = \begin{pmatrix} N \\ (M_r + M_r)^{-1} ((C_r + C_r) + (g_r + g_r) \hat{f}_r) \end{pmatrix}; \quad (36)$$

$$G_u(x) = \begin{pmatrix} O_{n \times s} \\ (M_r + M_r)^{-1} B_r \end{pmatrix}; \quad (37)$$

and we have the terms

$$M_r := N^T J^T \hat{M} J N; \quad (38)$$

$$C_r := N^T J^T \hat{M} J N + N^T (J^T \hat{M} J N + N^T J^T \hat{C} J N); \quad (39)$$

$$g_r := N^T J^T \hat{g}; \quad \hat{f}_r := N^T J^T \hat{f}; \quad (40)$$

Let us separate the nominal dynamics from the terms involving uncertainties and disturbances in (35). Applying the partially linearizing feedback in (11) and the input-output linearization feedback in (25) to the system in (35) and substituting

$$\begin{aligned} &= F^{-1} y; \\ &= \sum_{j=1}^{X^b} \frac{\partial F^{-1}}{\partial y_j} N F^{-1} y_j + F^{-1} y; \end{aligned} \quad (41)$$

the resultant uncertain closed loop input-output map becomes

$$y = (q; \gamma)^{-1} (u + (q; q; \gamma)); \quad (42)$$

where, F_j^{-1} refers to the j^{th} column of the matrix F^{-1} , y_j refers to the j^{th} component of output velocity and

$$:= I_{b \times b} + F M_r^{-1} M_r F^{-1}; \quad (43)$$

$$:= FM_r^{-1} (M_r X^0 @ F^{-1} NF^{-1} Y_j - C_r F^{-1} y - g_r + \delta_r); \quad (44)$$

Assumption 9. We assume the bound $FM_r^{-1} M_r F^{-1} < 1 < \frac{1}{1+\frac{1}{2}}$, where the operator $\| \cdot \|$ denotes the square Frobenius norm of a matrix and δ is a constant real number.

Assumption 10. In many applications of the developed theory, the dimension of the output $n = m = 2$. Examples include different types of autonomous rovers, under water or aerial vehicles moving in a plane. Therefore, we assume in the rest of the paper. With some extra work, the analysis presented in this paper may be extended to higher dimensional outputs.

Problem2 (LQR Control Problem) In system (47) find the control input $v_{eq}(t)$ to asymptotically stabilize the origin for y_e , while reaching the origin in a pre-specified finite time t_f and minimizing the following performance measure functional,

$$J(v_{eq}(t); e(t)) = \frac{1}{2} \int_0^{t_f} v_{eq}^T K_v v_{eq} + e^T K_e e \, dt; \quad (48)$$

where K_v and K_e are both 2×2 positive definite diagonal weighting matrices. The solution can be found based on the variational principle. We first form the Hamiltonian function H as:

$$H(v_{eq}; y_e; p) = v_{eq}^T K_v v_{eq} + e^T K_e e + p^T y_e(v_{eq}; y_e); \quad (49)$$

Consequently based on Assumption 9 and 10, the determinant of matrix \mathcal{H} is always strictly positive. Hence, this matrix is always invertible and its diagonal elements are strictly positive. The state-space representation of the error-dynamics of the uncertain mapping in (42) becomes:

$$\dot{e} = (q;)^{-1} (v + e(q; ; e; t)); \quad (45)$$

where $e = y - y_d$, and $e = (I -) y_d$.

Assumption 11. $k_e k < 2$, where 2 is a constant real number.

Sliding mode control as a variable structure control method can be applied to the system in (45) to stabilize the tracking error of the output, which guarantees robustness against bounded uncertainties. The design of SMC is performed in two steps:

(i) designing the sliding manifold on which error becomes asymptotically stable towards the origin, (ii) designing a switching control law pushing a system outside of the sliding manifold towards it. Accordingly, the control law designed based on SMC consists of an equivalent control input denoted by the 2-dimensional vector v_{eq} associated with the motion on the sliding manifold, and a switching control law denoted by the 2-dimensional vector v_s , i.e.,

$$v = v_{eq} + v_s; \quad (46)$$

A. Optimal Sliding Manifold Design

The sliding manifold determines the convergence behaviour of the output error to zero, when the system operates in nominal conditions (with no uncertainties and disturbances). Considering the nominal linearized input-output map in (26) along with an integral action to eliminate steady state error and improve robustness, the state space representation of the error dynamics becomes:

$$\dot{y}_e = A_c^3 y_e + B_c^3 v_{eq}; \quad (47)$$

where

$$y_e := \int_0^{t_f} e^T(\cdot) \, d\tau \quad e^T \underline{e}^T \in \mathbb{R}^6;$$

and $A_c^3 \in \mathbb{R}^{6 \times 6}$ and $B_c^3 \in \mathbb{R}^{6 \times 2}$ are the constant matrices representing the canonical form of a chain of three integrators.

where the 6-dimensional vector p is a vector of Lagrange multipliers, i.e., co-states, and the functionality \mathcal{H} is in (47). The necessary conditions for the optimal trajectory and the optimal control input beside the constraint coming from the error dynamics in (47) are [36]:

$$p = \frac{\partial H}{\partial y_e}(y_e; v_{eq}; p); \quad (50)$$

$$0 = \frac{\partial H}{\partial v_{eq}}(y_e; v_{eq}; p) \quad v_{eq} = K_v^{-1} O_{2 \times 4} I_{2 \times 2} p; \quad (51)$$

where the superscript asterisk refers to the optimal curves. Substituting v_{eq}^* in (47) and (50), the 12 number of linear first order ordinary differential equations known as the reduced state co-state equations become:

$$\dot{x}_{ep} = A_L x_{ep}; \quad (52)$$

where the 12-dimensional vector $x_{ep} = [(y_e)^T; (p)^T]^T$ and $A_L \in \mathbb{R}^{12 \times 12}$ is a constant matrix (see Appendix I). The solution of this equation is

$$x_{ep} = B_L(t) x_{ep}(t_0); \quad (53)$$

where $B_L = \exp(A_L t)$ is the state transition matrix.

Let $B_{Lf} = B_L(t_f)$, which can be partitioned as

$$B_{Lf} = \begin{bmatrix} B_{Lf}^{1;1} & B_{Lf}^{1;2} \\ B_{Lf}^{2;1} & B_{Lf}^{2;2} \end{bmatrix}; \quad (54)$$

where $B_{Lfi;j} \in \mathbb{R}^{6 \times 6}$ ($i, j = 1; 2$). Considering the split boundary value conditions $p_e(t_f) = 0$ and $y_e(0) = y_e$, the optimal control input v_{eq}^* is obtained in the form of a PID controller. We set the equivalent control input v_{eq} as

$$v_{eq} = v_{eq} = K_I K_p K_d y_e; \quad (55)$$

where the matrix of optimal gains is:

$$K_I K_p K_d = K_v^{-1} O_{2 \times 4} I_{2 \times 2} B_{Lf}^{-1} B_{Lf}^{1;1}; \quad (56)$$

The matrix $B_{Lf}^{1;2}$ based on the structure of matrix A_L is invertible (see Appendix I). The obtained control law in (55) results in the convergence of the error on the following manifold

$$e + K_d \underline{e} + K_p e + K_I \int_0^t e(\cdot) \, d\tau = 0; \quad (57)$$

Integrating this manifold, the following \bar{q} -dimensional relative degree one sliding manifold is designed:

$$s = \underline{e} + K_d \underline{e} + K_p \int_0^t \underline{e}(\tau) d\tau + K_I \int_0^t \int_0^{\tau} \underline{e}(\sigma) d\sigma d\tau = 0; \quad (58)$$

B. Switching Control Law

After designing an optimal sliding manifold, the switching control law v_s is obtained based on the uncertain error dynamics in (45), such that the sliding manifold $s = 0$ is attractive in finite time. Let us define the function (y_e) and the constant k_0 as

$$(y_e) := \frac{(p\bar{2} + 1)(k_{v_{eq}}k + 2) + k_{v_{eq}}k}{1}; \quad (59)$$

$$k_0 := \frac{1}{1}; \quad (60)$$

Theorem 1. For any function satisfying the condition

$$(y_e) \frac{1}{1} - p\bar{2} + k_0 > 0; \quad (61)$$

where k_0 is a strictly positive arbitrary constant, the switching control law,

$$v_{si} = \text{sgn}(s_i) \quad (62)$$

makes the system in (42) asymptotically stable towards the optimal sliding manifold in (58) as long as $FM_r^{-1} M_r F^{-1} < 1 < \frac{1}{1+p\bar{2}}$ and $k_{e_k} < 2$.

Proof: Prior to providing the stability proof of the proposed switching control law, let us remind some important properties of the matrix A . Based on Assumptions 9, 10, and 11, we have:

- (i) Due to triangle inequality, $p\bar{2} - 1 < k < p\bar{2} + 1$.
- (ii) Decomposing A into matrices of its diagonal elements s_d and its off-diagonal elements s_o , i.e., $A = s_d + s_o$, it can be deduced that $k_o k < 1$, and the diagonal elements of s_d are strictly positive.
- (iii) The determinant of A is strictly positive.
- (iv) Since A is two by two, $\det(A) = \frac{k_o k}{\det(A)}$.
- (v) The matrix A^{-1} can be also decomposed into the matrices of its diagonal elements s_d^{-1} and its off-diagonal elements s_o^{-1} , i.e., $A^{-1} = s_d^{-1} + s_o^{-1}$. Since A is two by two, it can be deduced that $s_o^{-1} = \frac{k_o k}{\det(A)}$ and $s_d^{-1} = \frac{k_d k}{\det(A)}$.

For stability proof, we consider the following positive definite function as a Lyapunov candidate

$$V(s) = \frac{1}{2} s^T s; \quad (63)$$

The time derivative of V is

$$\dot{V} = s^T \dot{s} = s^T [A^{-1}(v_s + v_{eq} + e) + v_{eq}]; \quad (64)$$

using the definition of the sliding surface in (58) and in (55), and the uncertain error dynamics in (45). We write

$\dot{V} = \dot{V}_1 + \dot{V}_2$, where $\dot{V}_i = s_i \dot{s}_i$, for $i = 1; 2$. Decomposing the matrix A^{-1} into the matrices of its diagonal elements s_d^{-1} and its off-diagonal elements s_o^{-1} , (64) becomes:

$$\dot{V} = s^T s_d^{-1} v_s + s^T s_o^{-1} v_s + s^T [A^{-1}(v_{eq} + e) + v_{eq}]; \quad (65)$$

Hence,

$$\dot{V}_i = s_i s_{di}^{-1} v_{si} + |s_i| j(s_o^{-1} k_{v_s} k + s_{di}^{-1} (k_{v_{eq}} k + k_{e_k}) + k_{v_{eq}} k); \quad (66)$$

where s_{di}^{-1} refers to the i th diagonal element of matrix s_d^{-1} , and s_i denotes the i th component of vectors. Since s_{di}^{-1} is a positive number,

$$\frac{\dot{V}_i}{|s_i|} = s_i v_{si} + |s_i| j \left[\frac{s_o^{-1} k_{v_s} k}{s_{di}^{-1}} + |s_i| j \frac{s_o^{-1} (k_{v_{eq}} k + k_{e_k}) + k_{v_{eq}} k}{s_{di}^{-1}} \right]; \quad (67)$$

Considering the norm inequality for a diagonal element of A , i.e., $1 - 1 < s_{di}^{-1}$, and based on property (v) for the matrix A , an upper bound for the right hand side of (67) is obtained by substituting a lower bound of the denominators.

$$\begin{aligned} \frac{\dot{V}_i}{|s_i|} &= s_i v_{si} + |s_i| j \frac{\det(A)}{1} \frac{s_o^{-1} k_{v_s} k}{s_{di}^{-1}} \\ &+ |s_i| j \frac{\det(A)}{1} \frac{s_o^{-1} (k_{v_{eq}} k + k_{e_k}) + k_{v_{eq}} k}{s_{di}^{-1}} \\ &= s_i v_{si} + |s_i| j \frac{k_o k_{v_s} k}{1} \\ &+ |s_i| j \frac{k_o k (k_{v_{eq}} k + k_{e_k}) + k_{v_{eq}} k}{1}; \quad (68) \end{aligned}$$

Based on properties (i) and (ii) for the matrix A and Assumption 11, an upper bound for the right hand side of (68) is obtained by substituting the upper bounds of the nominators. According to (59) and (60) we have

$$\begin{aligned} \frac{\dot{V}_i}{|s_i|} &= s_i v_{si} + |s_i| j \frac{1 k_{v_s} k}{1} \\ &+ |s_i| j \frac{(p\bar{2} + 1)(k_{v_{eq}} k + 2) + k_{v_{eq}} k}{1} \\ &= s_i v_{si} + |s_i| j (1 + k_0 k_{v_s} k); \quad (69) \end{aligned}$$

Substituting v_{si} from (62) and considering the fact that $k_{v_s} k < \frac{1}{2}$, we obtain

$$\begin{aligned} \frac{\dot{V}_i}{|s_i|} &= s_i \text{sgn}(s_i) + |s_i| j (1 + p\bar{2} k_0) \\ &= |s_i| j (1 - (1 + p\bar{2} k_0)); \quad (70) \end{aligned}$$

Since based on Assumption 9, $p\bar{2} k_0 > 0$, it can be deduced from (61) that $(1 - (1 + p\bar{2} k_0)) < 0$. Hence,

$$\frac{\dot{V}_i}{|s_i|} = |s_i| j (1 - (1 + p\bar{2} k_0)) < 0; \quad (71)$$

Since $\dot{V} = \dot{V}_1 + \dot{V}_2$, the inequality in (71) guarantees that \dot{V} is negative definite under the assumptions of the theorem and

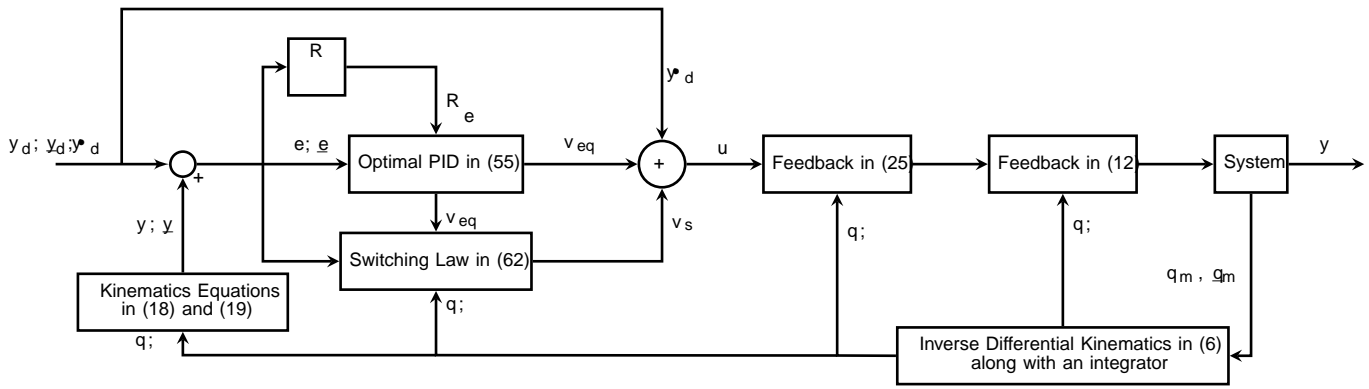


Fig. 1: Optimal output-tracking sliding mode control block diagram

the closed-loop system is stable towards the sliding manifold $s = 0$.

To alleviate the chattering effects, the switching control law (62) can be approximated by a high slope continuous saturation function

$$v_{si} = (y_e) \text{sa}\left(\frac{s_i}{\delta}\right); \quad (72)$$

where for a constant $\delta < 1$

$$\text{sa}\left(\frac{s_i}{\delta}\right) := \begin{cases} 1 & s_i < -\delta \\ \frac{s_i}{\delta} & -\delta < s_i < \delta \\ -1 & s_i > \delta \end{cases}$$

Based on the switching control law in (72), the two components of the Lyapunov function V , i.e., V_1 and V_2 , satisfy the following inequality instead of (69):

$$\frac{V_i}{di} \leq -s_i \text{sa}\left(\frac{s_i}{\delta}\right) + |s_i|j \quad (73)$$

Clearly in the region where $|s_i| \leq \delta$ (for $i = 1; 2$), the inequality (71) still holds; and hence the system in (42) reaches the boundary layers $|s_i| = \delta$ (for $i = 1; 2$) around the optimal sliding manifold (58) in finite time and remains inside thereafter.

Remark7. Inside of the boundary layers $|s_i| \leq \delta$ (for $i = 1; 2$) around the optimal sliding manifold, the vector s is bounded and reaches a positively invariant set in finite time. This leads to tracking with a guaranteed precision which can be arbitrarily adjusted by choosing [16], [33].

The block diagram of the proposed control strategy depicted in Fig. 1, where the vectors q_m and \dot{q}_m are the set of measurable generalized coordinates and velocities. The states and the outputs of the system that are not measurable can be computed using the inverse differential kinematics relationship in (6) based on the nonholonomic constraints and the kinematics equations in (18) and (19), respectively.

Remark8. If $s > n - m$, i.e., if the system contains redundant control directions, the matrix in (11) is not a square invertible matrix. Accordingly, specifying the vector of control inputs to accomplish a control task does not result in a unique solution for the control inputs in (8). In this paper, the right pseudo-inverse algorithm is employed to find

a solution for u that minimizes the quadratic norm of the control actions.

Remark9. If the system starts its motion with an initial error, it might be far from the optimal sliding manifold in (58). This can result in producing large amounts of control actions by the proposed switching control law at the beginning of the motion. This drawback can be rectified by properly setting initial values for the integral or double integral terms in (58) in order for the system to start its motion on the sliding manifold.

V. IMPLEMENTATION ON A SIX-WHEEL TYPE (1; 1) AUTONOMOUS LUNAR ROVER

In this section, the developed theory is implemented on a Lunar six-wheel type (1; 1) autonomous rover. Type (1; 1) autonomous rovers is referring to the category of such systems whose motion in only one direction (forward/backward) can be directly controlled and their orientation is indirectly controlled during the forward/backward motion through a single steering command [37].

Remark10. In type (1; 1) autonomous rovers, system may contain more than one steering degree-of-freedom, but to ensure mobility of the system axes of rotations of all steerable wheels must intersect at the center of turning (Ackerman Condition). See Fig. 2. This results in holonomic constraints between steering degrees of freedom and hence system indirectly rotates by a single steering command.

The system under study can be modelled as the composition of a main body which is the most massive part of the rover and six driven wheels located on three parallel axes and connected to the main body by ideal joints. Wheels located on centre and side axes can only have axial rotation while the front wheels are allowed to have both steering and axial rotation relative to the main body. To each part, a body-fixed coordinate frame is assigned. For the main body, the origin of the coordinate frame is located at the middle of the center wheels' axis, its x-axis

is aligned with the rover's forward direction of motion and its y-axis is in the lateral direction pointing towards the port side (xy-frame). For the wheels, the assigned body coordinate frames are located at the centre of the wheels and their axes are parallel to those of main body frame when axial rotation and steering angles are all equal to zero. The schematic of the

system is depicted in Fig. 2, where x_0y_0 -frame is the inertial coordinate frame, the vector $[x_{cm} \ y_{cm}]^T$ denotes the position of the main body's centre of mass in xy -frame, $2c$ is the lateral distance between the wheels, and L_0 are respectively the longitudinal distances between the front and rear wheels from the origin of xy -frame. Further, the radius of the wheels is denoted by R_w . Assuming that the system only has planar

Remark 11. Since the center wheels are always parallel, their corresponding no-lateral velocity constraints are linearly dependent. Hence, to include both constraints only one equation is considered when forming \hat{A} . Further, since the steering angles are assumed to satisfy the Ackerman condition, the no-lateral velocity constraint at the starboard front wheel is linearly dependant on the second and third rows of \hat{A} , hence it is excluded, when forming \hat{A} .

Based on the Lagrange d'Alembert principle, the equations of motion of the rover are derived. The matrices $\hat{A}(\mathbf{q})$ and $\hat{C}(\mathbf{q}; \dot{\mathbf{q}})$ in (2) are obtained and presented in Appendix II. Assuming that only planar motion is allowed, the vector $\mathbf{g} = \mathbf{0}$. The vector of control inputs consists of the torques applied to all wheels collocated to their axial motion along with the steering torques applied to the front wheels, i.e., $\dim(\mathbf{u}) = s = 8$ and the matrix of control directions is

$$\hat{B} = \begin{bmatrix} \mathbf{0}_{8 \times 3} & \mathbf{I}_{8 \times 8} \end{bmatrix}^T \quad (77)$$

Based on the imposed constraints, one possible everywhere nonsingular choice of matrix \hat{N} is:

$$\hat{N} = \begin{bmatrix} \frac{R_w}{L} \cos(\rho) (L \cos(\rho) + c \sin(\rho)) & 0 & 0 & 0 & 0 & 0 & 0 & 0 \\ \frac{R_w}{L} \sin(\rho) (L \cos(\rho) + c \sin(\rho)) & 0 & 0 & 0 & 0 & 0 & 0 & 0 \\ \frac{R_w}{L} \sin(\rho) & 0 & 0 & 0 & 0 & 0 & 0 & 0 \\ 0 & 0 & 0 & 0 & 0 & 0 & 0 & 0 \\ \cos(\rho) & 0 & 0 & 0 & 0 & 0 & 0 & 0 \\ \frac{2c}{L} \sin(\rho) + \cos(\rho) & 0 & 0 & 0 & 0 & 0 & 0 & 0 \\ \cos(\rho) & 0 & 0 & 0 & 0 & 0 & 0 & 0 \\ \frac{2c}{L} \sin(\rho) + \cos(\rho) & 0 & 0 & 0 & 0 & 0 & 0 & 0 \\ 1 & 0 & 0 & 0 & 0 & 0 & 0 & 0 \\ 0 & 0 & 0 & 0 & 0 & 0 & 0 & 1 \end{bmatrix} \quad (78)$$

Fig. 2: schematic of the system

motion, the configuration manifold of the system $\hat{Q} = \mathbb{R}^2 \times \mathbb{T}^9$ (Cartesian product of \mathbb{R}^2 and 9-torus) is 11 dimensional, i.e., $\dim(\hat{Q}) = 11$, and the generalized coordinates of the system are

$$\mathbf{q} = [x_b \ y_b \ \theta_s \ \theta_p \ \alpha_1 \ \alpha_2 \ \alpha_3 \ \alpha_4 \ \beta_1 \ \beta_2 \ \beta_3 \ \beta_4]^T \quad (74)$$

Here, $[x_b \ y_b \ \theta]^T \in \mathbb{R}^3$ is the position and orientation of xy -frame from x_0y_0 -frame and expressed in the inertial frame, $\theta_s; \theta_p \in \mathbb{T}^1$ are respectively the rotation of the starboard and port front wheels, $\alpha_1; \alpha_2 \in \mathbb{T}^1$ are the steering angle of the starboard and port front wheels, respectively, and $\beta_1; \beta_2; \beta_3; \beta_4 \in \mathbb{T}^1$ refer to the axial rotations of port center wheel, starboard center wheel, port rear wheel, and starboard rear wheel, respectively.

The imposed constraints on the system are (i) a constraint between steering angles of the front wheels due to the Ackerman condition, and (ii) the no longitudinal and lateral slip condition at all wheels, except rear wheels. Considering the rover's mobility, the no-lateral velocity constraint at the rear wheels is relaxed in this paper, and they are assumed to skid-steer.

Accordingly, the number of everywhere linearly independent constraints is $s = 9$ and the constraint matrix \hat{A} is formed as in (75). The first row of \hat{A} captures the constraint between the steering degrees of freedom, where

$$s = f_A(\rho) = \tan^{-1} \left(\frac{\tan(\rho)}{1 + \frac{2c \tan(\rho)}{L}} \right); \quad (76)$$

The second and third rows of \hat{A} refer to the no-lateral velocity constraint at the wheel-ground contact point of the port front wheel and the center wheels, respectively. The remaining rows of \hat{A} correspond to the no-longitudinal velocity constraint at the wheel-ground contact point of all six wheels.

where

$$\hat{N}_{4,1} = \sin(\rho) \left(\frac{2c}{L} \cos(\theta_s) + \sin(\theta_s) \right) + \cos(\rho) \cos(\theta_s);$$

$$\hat{N}_{5,2} = \frac{L^2}{2c^2 + L^2 - 2cL \sin(2\rho)};$$

To investigate the nonholonomicity of the constraints in (75), the involutive closure of the distribution $\mathcal{D} = \text{im}(\hat{N})$ needs to be calculated. Let us form the distribution $\mathcal{D}_1 = \text{span}\{\hat{N}_1; \hat{N}_2; n_1; n_2; n_3\}$ where \hat{N}_1 and \hat{N}_2 respectively are the first and the second column of \hat{N} and $n_1 = L_{\hat{N}_1} \hat{N}_2$. The Lie derivative $L_{\hat{N}_1} \hat{N}_2$ is calculated based on (14) and it is verified to be linearly independent of \hat{N}_1 and \hat{N}_2 using Wolfram Mathematica Symbolic Software. Note that the final form of the calculated Lie derivatives are excluded due to space constraints. Similarly, in the next step, the distribution $\mathcal{D}_2 = \text{span}\{\hat{N}_1; \hat{N}_2; n_1; n_2; n_3; n_4\}$ is formed where $n_2 = L_{\hat{N}_1} n_1$ and $n_3 = L_{\hat{N}_2} n_1$ which is of dimension 5. Finally, following the same pattern, the 7-dimensional distribution $\mathcal{D}_3 = \text{span}\{\hat{N}_1; \hat{N}_2; n_1; n_2; n_3; n_4; n_5\}$ is calculated where

$$F = \begin{bmatrix} \frac{2R_w}{L}(\cos(\rho) + \sin(\rho)) & \sin(\rho) & \sin(\rho) \\ \frac{2R_w}{L}(\sin(\rho) + \cos(\rho)) & \sin(\rho) & \cos(\rho) \end{bmatrix} \quad (88)$$

where $\rho > 0$ is the distance between the look-ahead point and the center of port front wheel and is substituted from (83). With this choice of output the determinant of the decoupling matrix F is equal to R_w and it is everywhere full rank. Therefore, the system is input-output linearizable applying static state feedbacks in (11) and (25).

Proposition 6 (observability) For the system under study, considering the state space representation in (9) and output in (87), the axial rotation of both front wheels, ρ along with the summation of the axial rotation of the center wheels $\rho_1 + \rho_2$ are locally unobservable at all states.

Proof: Let S be a family of nonsingular involutive co-distributions, being invariant under the drift vector field $f(x)$ and the columns of $G(x)$ in (9) and they contain the span of exact co-vector fields corresponding to the components of the output in (87):

$$G_0 := \text{span} \left\{ \left(\frac{\partial y_1}{\partial x} \right)^T; \left(\frac{\partial y_2}{\partial x} \right)^T \right\} \quad (89)$$

The set of co-distributions S has a minimal element [32]. We denote the minimal element of S by S_0 and its involutive annihilator distribution by S_0^\perp . At each state $x_0 \in X$ there is an open neighbourhood $U_0 \subset X$ of x_0 on which the integral of S_0^\perp defines a foliation of largest possible embedded slices with dimension equal to that of S_0^\perp in U_0 containing the unobservable states from the output in (87).

To construct S_0 for the system under study based on (9) and (87), first the co-distribution G_0 is formed. Since y is only a function of q , the Lie-bracket of any co-vector field in G_0 with respect to columns of $G(x)$ remains in G_0 and hence G_0 is invariant under the columns of $G(x)$. Then, the invariance condition of elements of S_0 under the drift vector field is checked. For the first basis element of this condition results in the co-distribution G_1 :

$$G_1 = G_0 + \text{span} \left\{ L_f \left(\frac{\partial y_1}{\partial x} \right)^T \right\} \quad (90)$$

where

$$L_f \left(\frac{\partial y_1}{\partial x} \right)^T = f^T \left(\frac{\partial^2 y_1}{\partial x^2} \right)^T + \left(\frac{\partial y_1}{\partial x} \right)^T \frac{\partial f}{\partial x} \quad (91)$$

For the system under study this Lie derivative is calculated using Wolfram Mathematica and the result is a co-vector field that is always transverse to G_0 . Therefore, G_1 is of dimension 3. Repeating the same procedure for the second basis element of G_0 , we obtain the four dimensional co-distribution G_2 :

$$G_2 = G_1 + \text{span} \left\{ L_f \left(\frac{\partial y_2}{\partial x} \right)^T \right\} \quad (92)$$

Based on the normal form in (29), we have at least 4 observable states, i.e., output and its velocity, which is consistent with what we have found so far. Imposing the involutivity condition, the co-distribution S_0 is obtained as the involutive closure of G_2 . Calculating G_2 and its involutive closure using

Wolfram Mathematica software, the annihilator distribution of S_0 at non-zero velocity states of the system is obtained as

$$S_0^\perp = \begin{bmatrix} 0 & 0 & 0 & 1 & 1 & 0 & 0 & 0 \\ 0 & 0 & 0 & 0 & 0 & 1 & 0 & 0 \\ 0 & 0 & 1 & 0 & 0 & 0 & 0 & 0 \end{bmatrix} \quad (93)$$

To obtain the unobservable states, the distribution S_0^\perp needs to be integrated. Hence, the unobservable states are $z_2; \rho; s; g$.

The dimension of the co-distribution S_0 for the system under study based on the state space representation in (9) along with the output in (87), differs at different states of the system. For example, when the system is stationary the dimension of S_0 is 4, i.e., the system contains 4 = 5 unobservable states (only output and its velocities are observable). However, the maximum dimension of S_0 is 6 indicating that regardless of the state, the system always has at least 3 unobservable states identified earlier.

To construct the normal form state space representation in (31) for the system under study, including the observability decomposition of the internal dynamics, we introduce

$$z = \begin{bmatrix} z_1 \\ z_2 \\ z_3 \\ z_4 \\ z_5 \\ z_6 \\ z_7 \\ z_8 \\ z_9 \end{bmatrix} = \begin{bmatrix} \frac{R_w}{2c}(\rho_2 - \rho_1) \\ \rho \\ s \\ p \\ \rho \\ z_6 \\ z_7 \\ z_8 \\ z_9 \end{bmatrix}, \quad \text{and} \quad (94)$$

This set of internal states is selected for simplicity and better indication of the system's performance. It can be verified that this set satisfies the condition in (28) and the resulting state transformation T is a diffeomorphism. Accordingly, the functions f^u and f^o in (31) for the system under study are

$$f^u = N^u(\rho) F^{-1} \begin{bmatrix} z_8 \\ z_9 \end{bmatrix}; \quad f^o = N^o(\rho) F^{-1} \begin{bmatrix} z_8 \\ z_9 \end{bmatrix}; \quad (95)$$

where

$$N^o = \begin{bmatrix} \frac{2R_w \sin(\rho)}{L} \\ 0 \\ 1 \end{bmatrix}; \quad N^u = \begin{bmatrix} \frac{2R_w}{L} \sin(\rho) + 2 \cos(\rho) \\ 1 \\ 0 \end{bmatrix} \quad (96)$$

The tracking-error zero dynamics corresponding to z_0 is formed as:

$$\dot{z}_e = \rho_e z_{8d} - z_{9d} F^{-1} \begin{bmatrix} -\dot{\rho}_d & -\dot{p}_d \end{bmatrix}^T; \quad (97)$$

where ρ_e and p_e respectively refer to the error in ρ and p , and $z_{8d}, z_{9d}, \dot{\rho}_d$, and \dot{p}_d denote the desired velocities of the output, ρ , and p , respectively. Applying Lyapunov's indirect method, it is proved that based on this choice of output for type 1 error dynamics of z_1^o is asymptotically stable, if the system moves in forward direction, and it is unstable during backward motion [30].

Assumption 13. In this paper, we assume that the Lunar autonomous rover only moves in forward direction, and hence z_1^o is asymptotically stable towards origin.

Remark 12. Since for the Lunar rover the dynamics of z_1^o and z_2 , and z_{2e} and z_{1e}^o are asymptotically stable due to the proposed output-tracking

control law in (46) and Assumption 13, respectively, the error dynamics $\dot{z}_e \neq 0$ while $t \neq 1$; and hence z_e^u is bounded.

For this case study, we consider the following uncertainties in the inertia parameters: (i) an unknown constant mass with a bounded time-varying unknown moment of inertia about the z -axis (out of the plane of motion) $I_{z1}(t)$ that moves with a bounded unknown time varying trajectory $(x_1(t), y_1(t))^T$ in the main body's xy -frame, (ii) an unbalanced port center wheel modeled as an unknown bounded time-varying added mass m_u to the wheel at an unknown constant radius R_u . In terms of disturbances, we consider an unknown bounded time-varying friction force with the magnitude of $f_r \operatorname{sgn}(\dot{y})$ that is applied on the rear wheels in the lateral direction. Accordingly, the vector of uncertain parameters is formed as: $(t) = [m_l \ x_1 \ y_1 \ I_{z1} \ m_u \ R_u \ f_r]^T$: As the result, the non-zero elements of the matrix $\hat{M}(\cdot; \cdot; \cdot)$ are

$$\begin{aligned} \hat{M}_{1;1} &= \hat{M}_{2;2} = m_l + m_u; \\ \hat{M}_{1;3} &= \hat{M}_{3;1} = m_l x_1 \sin(\cdot) \quad (cm_u + m_l y_1) \cos(\cdot); \\ \hat{M}_{1;6} &= \hat{M}_{6;1} = m_u R_u \sin(\cdot_1); \\ \hat{M}_{2;3} &= \hat{M}_{3;2} = m_l x_1 \cos(\cdot) \quad (cm_u + m_l y_1) \sin(\cdot); \\ \hat{M}_{3;3} &= I_{z1} + c^2 m_u + m_l (x_1^2 + y_1^2); \\ \hat{M}_{3;6} &= \hat{M}_{6;3} = cm_u R_u \cos(\cdot) \sin(\cdot_1); \\ \hat{M}_{6;6} &= m_u R_u^2; \end{aligned} \tag{98}$$

The matrix $\hat{C}(\cdot; \cdot; \cdot; \cdot; \cdot)$ is then obtained as

$$\hat{C} = \frac{\partial \hat{M}}{\partial \dot{z}} + \frac{\partial \hat{M}}{\partial \dot{z}_1} + \sum_{i=1}^7 \frac{\partial \hat{M}}{\partial \dot{z}_i} + \begin{matrix} 2 & 3 \\ \text{O}_2 & \text{O}_3 \\ \text{O}_2 & \text{O}_3 \\ \text{O}_5 & \text{O}_5 \end{matrix} \begin{matrix} 11 \\ 11 \\ 11 \\ 11 \\ 11 \\ 11 \\ 11 \end{matrix} \begin{matrix} Z \\ Z \\ Z \\ Z \\ Z \\ Z \\ Z \end{matrix}; \tag{99}$$

where \dot{z}_i refers to the i^{th} element of \dot{z} . The vector of uncertain potential forces \hat{g} due to the unbalanced wheel is

$$\hat{g} = [O_{1 \ 5} \quad m_u g_u R_u \cos(\cdot_1) \quad O_{1 \ 5}^T]^T; \tag{100}$$

where g_u denotes the gravitational constant. Finally, the direction of the friction disturbance force is determined to be

$$\hat{J}_d = [\sin(\cdot) \quad \cos(\cdot) \quad L_0 \quad O_{1 \ 8}]; \tag{101}$$

Subsequent to determining the uncertain matrices \hat{M} and \hat{C} , the vector \hat{g} , and the row vector \hat{J}_d , the uncertain state-space representation in (35) can be formed for the Lunar autonomous rover and the proposed robust optimal output-tracking control law can be implemented.

A. Simulation Results

The Lunar autonomous rover system along with the proposed controller is modeled in MATLAB R2019b. We discretize our model in (8) with step-time equal to one millisecond and use Euler method for numerical integration. Table I depicts the values of the parameters used in the model of the system, modeled uncertainties, and the controller. The desired trajectory for the rover is considered that includes

Rover Parameters			
L [m]	L ₀ [m]	c [m]	R _w [m]
1	0.5	0.5	0.3
l [m]	x _{cm} [m]	y _{cm} [m]	m _r [Kg]
1	0.25	0	600
m _w [Kg]	J _r [Kg/m ²]	J _{wy} [Kg/m ²]	J _{wz} [Kg/m ²]
40	450	1.3	1
Uncertain Parameters			
m _l [Kg]	x _l [m]	x _l [m/s]	y _l [m]
250	0.5 cos (t=3)	0.16 sin (t=3)	0.3 sin (t=3)
y _l [m/s]	m _u [Kg]	m _u [Kg/s]	R _u [m]
0.1 cos (t=3)	0.1	0.025 cos (t=3)	0.125 sin (5t)
I _{z1} [Kg/m ²]	I _{z1} [Kg/m ² s]	f _r [N]	g _u [m/s ²]
75	20 cos (t=2)	140	1.636
Control Parameters			
K _v	K _e	t _f [s]	1
l _{2 \ 2}	l _{2 \ 2}	10	0.31
2		0	
1	0.55	0.0001	

TABLE I: Kinematic and dynamic parameters of the Lunar rover, uncertain parameters defined in the simulation, and control parameters

Fig. 3: Desired trajectory for the rover: (a) desired path (b) desired forward velocity of the rover (c) desired steering angles of port (black line) and starboard (blue line) front wheels

acceleration from zero velocities with 0.18 m/s^2 in the forward direction of motion for 100s and two steering commands for 10s and 40s. The desired initial value for the vector of generalized coordinates $z_d(0) = [L \ l \ c \ O_{1 \ 9}]^T$, such that the initial value of the desired output trajectory is zero. Following this desired trajectory, the origin of the xy -frame moves on a figure-eight path while it is continuously accelerating (see Fig. 3). Based on (87) the desired trajectory for the output is determined. Note that the designed trajectory has large velocities to highlight the effect of uncertainties at the output. Considering a desired trajectory with low-velocity profile reduces the Coriolis effects of the uncertainties and does not properly reflect the performance of the proposed control law.

Remark 13. For simplicity, the desired trajectory depicted in Fig. 3 is produced based on the commands for quasi-velocities \dot{z}_p and \dot{z}_ρ . That justifies the slight reduce in the velocity of the rover at 40th second of the simulation when a considerable change in the steering is applied and system enters another

circle with higher steering angle.

According to the weighting matrices K_v and K_e and the convergence time t_c reported in Table I, the matrix of optimal gains in (58) is obtained as:

$$[K_i \ K_p \ K_d] = \begin{bmatrix} 0.14 & 0 & 1.19 & 0 & 1.55 & 0 \\ 0 & 0.14 & 0 & 1.19 & 0 & 1.55 \end{bmatrix} :$$

The function in the switching control law (62) is selected using the equality condition in (61) to be

$$(y_e) = \frac{1}{1 - P} \frac{P}{2k_0} + 0; \quad (102)$$

where λ and k_0 are defined in (59) and (60), respectively. We assume that the rover starts its motion with zero velocity, an initial error $[0 \ 0.5]^T$ in the output, and at the configuration described by $x(0) = [L \ l \ c + 0.5 \ 0 \ 1 \ 9]^T$. To start the motion of the system on the optimal sliding manifold, we introduce an initial value for the integral of the error, based on (58).

The simulation is once conducted only with the proposed optimal PID control law obtained in (55) as part of the output-tracking SMC design. The results corresponding to this simulation are labeled by "OPID". The same scenario is simulated using the optimal output-tracking SMC with both v_{eq} in (55) and the switching control law in (72), whose results are labeled by "ORS". The errors in the trajectory tracking for the rover, the output and the steering angles are shown in Fig. 4. Further, the control torques at all wheels and the steering degrees of freedom are compared in Fig. 5.

Based on Fig. 4 in both control approaches, system is navigated from its initial location towards the desired trajectory and tracks it with an acceptable amount of error caused by the imposed uncertainties and disturbances. By acceptable error we mean less than half a meter maximum magnitude of the steady state error in the position of the rover during circling with a high velocity equal to 17.5 m/s . Since in the design of the optimal controller t_c is 10 s , the control system is in the steady state regime after 10 s . However, it is evident that adding the proposed switching control law (see Table I), the highest amplitude of chattering is observed improves the robustness of the controller and reduces the error to be near 5 N.m . When the system moves with a constant velocity (after time 100 s) on a circle since the center of mass is located ahead of the origin of the x -frame, both controllers are producing time-varying brake forces to compensate for the Coriolis effects. The low-frequency oscillations (with large amplitude) in the produced control actions by both control laws during circling are due to the sinusoidal changes in the location of the center of mass of the system. Throughout the motion, the system also experiences high-frequency oscillations (with small amplitude) in the produced control torques as the result of the unbalanced port center wheel. The period of the high-frequency oscillations decreases as the velocity of the system increases.

According to Fig. 5, the control actions produced by the ORS control scheme follow the same trend comparing with those obtained in the OPID case, with the addition of some chattering effects as the result of the proposed switching control law. The magnitude of the chattering can be adjusted by a proper choice of the variable. Generally, smaller results in smaller magnitude of errors but larger amplitude of chattering in control actions. Based on the adjusted variable for the steering angle, the highest amplitude of chattering is observed to be near 5 N.m . When the system moves with a constant velocity (after time 100 s) on a circle since the center of mass is located ahead of the origin of the x -frame, both controllers are producing time-varying brake forces to compensate for the Coriolis effects. The low-frequency oscillations (with large amplitude) in the produced control actions by both control laws during circling are due to the sinusoidal changes in the location of the center of mass of the system. Throughout the motion, the system also experiences high-frequency oscillations (with small amplitude) in the produced control torques as the result of the unbalanced port center wheel. The period of the high-frequency oscillations decreases as the velocity of the system increases.

VI. CONCLUSION

In this paper, mechanical systems subject to mixed holonomic and nonholonomic constraints in Pfaffan form were studied from various control perspectives, including reachability, feedback linearizability, and observability. Under

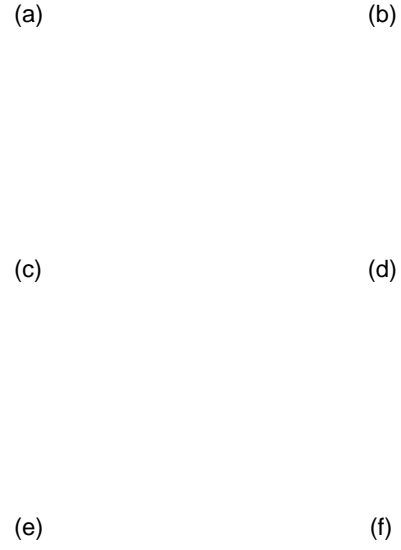


Fig. 4: Performance comparison of OPID and ORS in terms of error in (a) x_b , (b) y_b , (c) y_1 , (d) y_2 , (e) ρ , and (f) δ_s

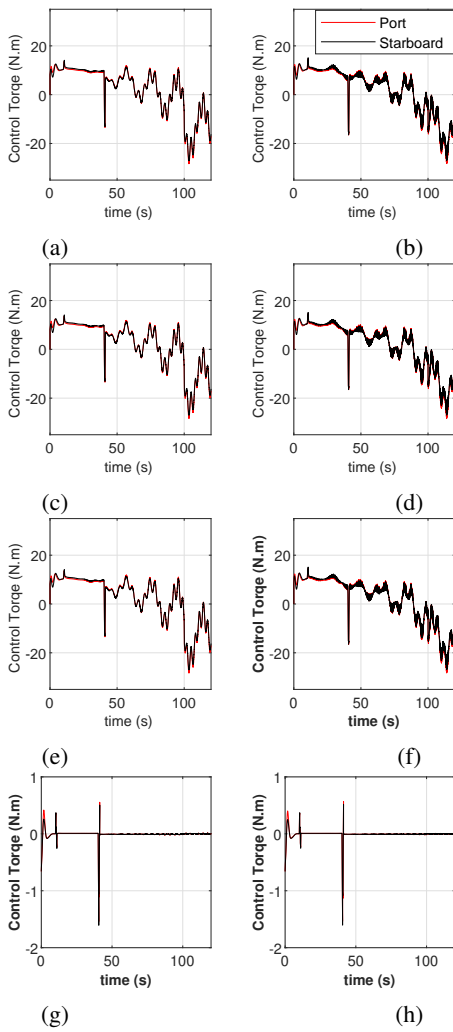


Fig. 5: Comparison of control commands generated by OPID (left) and ORS (right) laws. From the top to the bottom row, the plots respectively correspond to torques at the front wheels, center wheels, rear wheels, and steering degrees of freedom.

some conditions, the input-output linearization of such systems applying static state feedback was presented. Accordingly, we partitioned the states of the system into external states, and observable and unobservable internal states from the output of the control system before applying the linearizing feedback transformation. Such a partitioning of the states helps investigate the stability of the tracking error of the internal states that was demonstrated in the implementation phase. Including time-dependant bounded matched uncertainties in the inertia parameters and disturbance forces, the uncertain state-space representation of constrained mechanical systems was formulated. Applying the input-output linearizing feedback to the nominal plant, an output-tracking SMC algorithm was developed. We proposed an optimal design for the sliding manifold based on the finite-horizon LQR problem with splitting boundary value conditions. We also improved the performance of the switching control law in the optimal SMC by substituting the sign function with a high-slope saturation function and discussed its implications on the system's error

dynamics. The developed control law was used in the output-tracking control of a six-wheel autonomous Lunar rover, in a simulation environment. The results were compared with those obtained using the optimal PID control strategy. We showed that although the optimal PID demonstrated an acceptable performance in terms of both error and control actions, the addition of the proposed switching control law improved the error performance by one order of magnitude without considerably affecting the control actions.

Some possible future directions of this research are: (i) studying optimal distribution of the control actions when lifted to the unrestricted manifold, considering, e.g., traction of rover systems, and (ii) investigating the effects of violation of constraints, e.g., wheel slip in rovers, in the robust control design process.

APPENDIX I A_L AND B_L MATRICES

The nonzero elements of the constant matrix A_L in (52) are:

$$\begin{aligned} A_{L1,3} &= A_{L2,4} = A_{L3,5} = A_{L4,6} = 1; \\ A_{L5,11} &= \frac{1}{K_{v1,1}}; \quad A_{L6,12} = \frac{1}{K_{v2,2}}; \\ A_{L9,3} &= K_{e1,1}; \quad A_{L10,4} = K_{e2,2}; \\ A_{L9,7} &= A_{L10,8} = A_{L11,9} = A_{L12,10} = 1; \end{aligned}$$

where A_{Lij} refers to the element $(i;j)$ of the matrix A_L , K_{vij} denotes the element $(i;j)$ of the weighting matrix K_v , and K_{eij} denotes the element $(i;j)$ of the weighting matrix K_e . Choosing the weighting matrices K_v and K_e as the identity matrix, and selecting $t_f = 10s$ the determinant of the matrix $B_{LF1,2}$ is $1.54 \cdot 10^{12}$; and hence this matrix is well-conditioned.

APPENDIX II \hat{M} AND \hat{C} MATRICES

The nonzero elements of the matrix \hat{M} are:

$$\begin{aligned} \hat{M}_{1,1} &= \hat{M}_{2,2} = m_r + 6m_w; \\ \hat{M}_{1,3} &= \hat{M}_{3,1} = (2(L_0 - L)m_w - x_{cm}m_r) \sin(\cdot) - y_{cm}m_r \cos(\cdot); \\ \hat{M}_{2,3} &= \hat{M}_{3,2} = 2m_w(L - L_0) \cos(\cdot) + m_r(x_{cm} \cos(\cdot) - y_{cm} \sin(\cdot)); \\ \hat{M}_{3,3} &= 6(m_w c^2 + J_{wz}) + 2m_w(L^2 + L_0^2) + m_r(x_{cm}^2 + y_{cm}^2 + J_r); \\ \hat{M}_{3,5} &= \hat{M}_{5,3} = \hat{M}_{3,11} = \hat{M}_{11,3} = \hat{M}_{5,5} = \hat{M}_{11,11} = J_{wy}; \\ \hat{M}_{4,4} &= \hat{M}_{6,6} = \hat{M}_{10,10} = J_{wy}; \end{aligned}$$

where m_r is the mass of the main body, m_w is the mass of the wheels, J_r is the moment of inertia of the main body about the Z-axis (out of the plane) at its center of mass, J_{wy} denotes the moment of inertia of the wheels about their axes of rotation, and J_{wz} is the the moment of inertia of the wheels about the Z_0 -axis. Accordingly, based on the Lagrange d'Alembert principle, the matrix \hat{C} is obtained as

$$\hat{C}(\cdot; \dot{\mathbf{q}}) = \begin{pmatrix} @ \\ @ \\ @ \end{pmatrix} \dot{\mathbf{q}} + \begin{pmatrix} 0 & 11 & 2 \\ 1 & 2 & 8 \end{pmatrix} \frac{1}{2} (\dot{\mathbf{q}}^T @ \hat{M})^T \begin{pmatrix} @ \\ @ \\ @ \end{pmatrix}^T;$$

